Catalysis Today 259 (2016) 277–284

Contents lists available at ScienceDirect

Catalysis Today

journal homepage: www.elsevier.com/locate/cattod

Influence on nickel particle size on the hydrodeoxygenation of phenol over Ni/SiO_2

Peter M. Mortensen[a], Jan-Dierk Grunwaldt[b], Peter A. Jensen[a], Anker D. Jensen[a,*]

[a] Department of Chemical and Biochemical Engineering, Technical University of Denmark, Søltofts Plads, 2800 Kgs. Lyngby, Denmark
[b] Institute for Chemical Technology and Polymer Chemistry and Institute of Catalysis Research and Technology, Karlsruhe Institute of Technology, Engesserstrasse 20, 76131 Karlsruhe, Germany

ARTICLE INFO

Article history:
Received 17 December 2014
Received in revised form 24 June 2015
Accepted 11 August 2015
Available online 11 September 2015

Keywords:
Bio-oil
Heterogeneous catalysis
Hydrodeoxygenation (HDO)
Kinetics
Phenol
Structure sensitivity

ABSTRACT

Hydrodeoxygenation (HDO) of phenol over nickel nano-particles of different size (5–22 nm) supported on SiO_2 has been investigated in a batch reactor at 275 °C and 100 bar. Deoxygenation was only observed as a consecutive step of initial hydrogenation of phenol at the given conditions. Both the hydrogenation and deoxygenation reaction were found to be Ni-particle size dependent. Rapid hydrogenation of phenol to cyclohexanol was achieved over the catalysts with large particles, while the rate of deoxygenation of cyclohexanol was slow. For the catalysts with small Ni particles, the opposite behavior was observed Specifically, the turn over frequency (TOF) of hydrogenation was 85 times slower for 5 nm particles than for 22 nm particles. On the contrary, the TOF of cyclohexanol deoxygenation increased by a factor of 20 when decreasing the particle size from 20 nm to 5 nm. A simple kinetic model showed that the rate limiting step for phenol HDO shifted from deoxygenation to hydrogenation when the particle size was below 9–10 nm. Surface site population theory evidenced that the deoxygenation reactions were favored on step/corner sites, giving higher deoxygenation rates at small particles. For hydrogenation, the influence of particle size on the rate could be related to the size of the Ni facets with larger facets thus being better.

1. Introduction

Flash pyrolysis of biomass followed by hydrodeoxygenation (HDO) of the produced bio-oil has been identified as a prospective route for CO_2 neutral engine fuel production [1]. Through pyrolysis, practically any source of biomass can be converted into bio-oil [2]. Although much more energy dense than the original biomass, bio-oil has a low heating value compared to crude oil, a low shelf storage life, is viscous, and polar, making it unsuitable as an engine fuel. These characteristics are all associated with high contents of water and chemically bound oxygen in the bio-oil. However, as the oil has a higher volumetric energy density and is easy to handle relative to biomass it is more suitable for transport and further processing [1,3,4].

It would be advantageous if bio-oil can be upgraded to an oil similar to conventional crude oil using the HDO route, where hydrogen is used to remove the oxygen functionality in the bio-oil. This requires the presence of a catalyst, a temperature in the order of 200–400 °C, and typically a pressure of 70–200 bar [1].

Bio-oil consists of a vast number of oxygenated species and therefore many different reactions occur in HDO. It has been observed that a part of the oil (simple molecules such as short chain ketones) can easily be deoxygenated by direct removal of the oxygen functionality [5,6]. However, to deoxygenate more complex molecules, such as phenolics, an initial hydrogenation of the aromatic part of the molecule may be needed to make the oxygen group more susceptible for reaction with hydrogen [7]. Generally, phenol and phenolic derivatives are a fairly abundant part of bio-oil [8], which has been found as one of the more persistent oxy-compounds to deoxygenate [5,9]. This makes phenol an interesting model compound when investigating catalysts for HDO.

One of the major challenges in HDO is to find a suitable catalyst. Recent work has shown that nickel based catalysts have high activity for HDO reactions [10–17].

HDO of phenol over metallic catalysts and temperatures below 300 °C preferentially proceeds through a sequential reaction path as shown in Fig. 1, where hydrogenation of the aromatic ring takes place initially, producing cyclohexanone. This is rapidly hydrogenated to cyclohexanol. Deoxygenation of the cyclohexanol then

* Corresponding author.
E-mail address: aj@kt.dtu.dk (A.D. Jensen).

http://dx.doi.org/10.1016/j.cattod.2015.08.022
0920-5861/

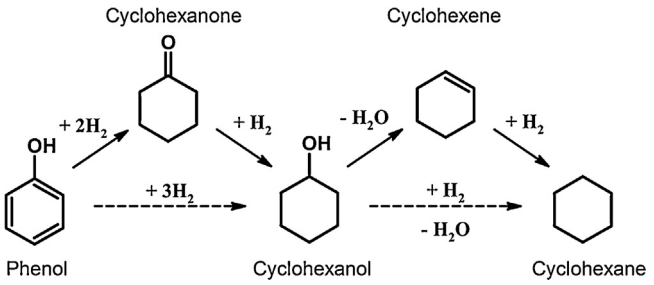

Fig. 1. Reaction scheme of HDO of phenol under mild conditions. Solid arrows indicate main pathways; while the dotted arrows indicate the steps of the kinetic model (see Section 2).

proceeds through either hydrogenolysis to cyclohexane or dehydration forming cyclohexene, which is readily hydrogenated into the final product cyclohexane [18,19]. This reaction path is fairly well established in the literature under mild conditions using noble metal/nickel catalysts. This mechanism has been reported, e.g., for HDO of phenol over Pd/C [20,21], Pt/C [22], Ni/HZSM-5 [23], Ni–MoS_2/Al_2O_3 [24], and nickel based catalysts [16,18].

In the current work HDO of phenol over Ni/SiO_2 catalysts has been investigated with special emphasis on understanding the influence of metal particle size and the relationship between the hydrogenation and deoxygenation reactions taking place for HDO of phenol.

2. Experimental

2.1. Catalyst synthesis

5 wt% Ni/SiO_2 was prepared by incipient wetness impregnation using $Ni(NO_3)_2{\cdot}6H_2O$ (Sigma–Aldrich, ≥97.0%) as precursor. Silica was supplied by Saint-Gobain NorPro, type SS6*138 with a purity of ≥99.5%, a specific surface area of 250 m^2/g, and a pore volume of 1.0 ml/g. Before impregnation, the SiO_2 was grinded to a particle size of 63–125 μm. The SiO_2 was impregnated with a 0.90 mol/l solution of $Ni(NO_3)_2{\cdot}6H_2O$ in water in one step. After impregnation, the sample was dried at 110 °C for 12 h.

In order to make catalysts with different particle size but same composition, the catalysts were pre-treated/calcined and reduced in different ways prior to the catalytic activity test:

- Red. 1: The catalyst was calcined initially at 400 °C in an oven and then reduced in the batch reactor at 395 °C (catalyst temperature) and 7 bar of H_2 in a stagnant gas atmosphere for 2 h. This method is expected to yield large nickel particles due to the high pressure and the presence of water [25–27].
- Red. 2: The catalyst was calcined initially at 400 °C in an oven and then reduced in the batch reactor with a flow of 1 Nl/min H_2 at 395 °C (catalyst temperature) and 5 bar of hydrogen for 2 h. This method is expected to yield intermediate size nickel particles since water is continuously removed.
- Red. 3: The catalyst was calcined initially at 400 °C in an oven and then reduced in a continuous flow reactor with a flow of 250 Nml/min H_2 and 250 Nml/min N_2 at 400 °C and 1 bar of hydrogen for 2 h and then transferred directly to the batch reactor. This method is expected to yield smaller nickel particles than Red. 2 due to the milder conditions and more controlled removal of water.
- Red. 4: Reduction of un-calcined $Ni(NO_3)_2/SiO_2$ in a continuous flow reactor with a flow of 250 Nml/min H_2 and 250 Nml/min N_2 at 400 °C and 1 bar for 2 h and then transferred directly to the batch reactor. This method is expected to yield small nickel particles, due to the direct reduction of the nickel nitrate catalyst precursor [28].

Temperature programmed reduction (TPR) data can be found in the ESI showing that complete reduction is achieved around 380 °C.

2.2. Catalyst testing

The experiments were performed in a 300 ml batch reactor from Parr (type 4566 of Hastelloy C steel). In an experiment 1 g of catalyst and 50 g of phenol (Sigma–Aldrich, ≥99%) were poured into the reactor. The mixture was stirred with a propeller at 380–390 rpm and heated to 275 °C in a hydrogen atmosphere, giving a final pressure of 100 bar. The heating rate was around 15 °C/min. During the experiments, hydrogen was added continuously to maintain the pressure of 100 bar. The experiments had a total reaction time of 5 h. To stop the experiment, the reactor was placed in an ice bath to cool the reactor within 5 min to room temperature. The start of the experiment was taken at the time when the heater was turned on (heating took ca. 20 min) and the end of the experiment was regarded as the time when the reactor was lowered into the ice bath. By threefold repetition of an experiment, it was found that this procedure had an uncertainty in the measured yields within ±2 mol%, corresponding to less than 5% as relative standard deviation. Overall there was a good repeatability of the experiments.

A blank experiment without catalyst with 10 g of phenol and 40 ml of H_2O at 275 °C and 100 bar for 4 h resulted in a conversion of only 0.3%, showing that the reactor was not catalytically active. Calculation of Mears' and Weisz–Prater criteria [29] indicated absence of mass transfer limitations in this system with the observed reaction rates. Details on the evaluation can be found in the ESI.

In some cases shorter experiments were performed to obtain conversions well below 100% for determination of kinetic parameters. For this purpose the batch reactor was initially heated without stirring, which decreased the rate of reaction to practically zero, until the desired temperature was reached. At this point the stirring was started at 380–390 rpm (start of experiment) and the reaction could be made at close to isothermal conditions. This allowed measuring the activity in short experiments of ca. 15 min.

2.3. Product analysis

Analysis of the liquid product was done with a Shimadzu GCMS/FID-QP2010UltraEi fitted with a Supelco Equity-5 column. The products were identified using a mass spectrometer (MS) and quantified with a flame ionization detector (FID). External standards were prepared for phenol, cyclohexanol, cyclohexanone, and cyclohexane. The concentrations of the remaining peaks were calculated from the FID on the basis of the effective carbon number method [30], where the concentration of a compound is found as:

$$C_i = C_{ref} \cdot \frac{A_i}{A_{ref}} \cdot \frac{\nu_{eff,ref}}{\nu_{eff,i}} \quad (1)$$

Here C is the concentration, A the area of the peak in the FID spectrum, and ν the effective carbon number. Index i refers to the compound with the unknown concentration and index ref refers to a reference compound where the concentration is known. In all calculations based on this formula cyclohexanol was used as reference. The effective carbon number was taken from the review by Schofield [30].

The conversion, X, was calculated as:

$$X = \left(1 - \frac{C_{Phenol} \cdot V_{final}}{n_{0,Phenol}}\right) \cdot 100\% \quad (2)$$

Here V_{final} is the final liquid volume and $n_{0,Phenol}$ the moles of phenol prior to reaction.

The yields (Y_i) of relevant products were calculated as:

$$Y_i = \frac{\nu_i \cdot n_i}{6 \cdot n_{0,Phenol}} \cdot 100\% \quad (3)$$

Here n_i is the moles of product i after reaction and ν_i is the number of carbon atoms in compound i.

The selectivity (S_i) of a compound (i) was calculated as:

$$S_i = \frac{Y_i}{X} \cdot 100\% \quad (4)$$

All calculations of X, Y_i, and S_i were corrected for loss of mass from transferring and filtration processes, which was quantified as the average of a number of blank tests.

2.4. Catalyst characterization

A Quantachrome iQ2 was used for measurement of the specific surface area using BET theory [31]. Nitrogen at its boiling point was used in the p/p_0 range from 0.05–0.3 to construct a seven point BET plot. The produced catalyst had a specific surface area of 210 m^2/g independent on preparation method.

Environmental transmission electron microscopy (ETEM) was performed using a Titan E-Cell 80-300ST TEM where images were obtained at reducing conditions. The samples were crushed, slurried with ethanol, and deposited on a copper grid covered with lacey carbon film. In the microscope these samples were heated to 450 °C and reduced in a flow of 5 Nml/min H_2 at a pressure of 2.5 mbar. The average nickel particle size was determined by measuring the size of >200 particles on the images and subsequently calculating the number based average.

Based on the ETEM determination of the average particle size, the dispersion (D) was calculated as [32]:

$$D = \frac{5.01 \cdot d_{M,at}}{d_M}, d_M > 6 \text{ nm} \quad (5)$$

$$D = \left(\frac{3.32 \cdot d_{M,at}}{d_M}\right)^{0.81}, 1 \text{ nm} < d_M < 6 \text{ nm} \quad (6)$$

Here $d_{M,at}$ is the atomic diameter of the relevant metal ($d_{Ni,at}$ = 2.48 Å) and d_M is the average particle size of the metal.

From the dispersion the number of surface sites can be determined as:

$$N_T = \frac{w_{Ni}}{M_{Ni}} \quad (7)$$

$$N_S = D \cdot N_T \quad (8)$$

Here N_T is the total number of nickel atoms on the catalyst, N_S is the number of surface atoms, w_{Ni} is the mass fraction of nickel on the catalyst, and M_{Ni} is the molar mass of nickel. This is later also used to calculate the turnover frequency (TOF) of the catalyst (cf. Section 3.2).

2.5. Kinetic model

We have previously shown [16] that the reaction scheme of Fig. 1 can be simplified to a system of only two reactions at the investigated conditions (development of the reaction scheme for the catalyst and derivation of the kinetic model is found in the ESI):

$$\text{Reaction 1}: \quad \text{Phenol} + 3H_2 \xrightarrow{k_1} \text{Cyclohexanol}$$

$$\text{Reaction 2}: \quad \text{Cyclohexanol} + H_2 \xrightarrow{k_2} \text{Cyclohexane}$$

Table 1
Overview of results from the 5 wt% Ni/SiO_2 catalysts with different particle sizes. d_{Ni} is the nickel crystallite size measured by ETEM, k_1 is the rate constant for hydrogenation, k_2 is the rate constant for deoxygenation, and ΔC is the deviation in the carbon balance. The experiments were made with 1 g of catalyst in 50 g phenol. T = 275 °C, P = 100 bar, reaction time = 5 h.

Sample	d_{Ni} [nm]	k_1 [ml/(kg_{cat} min)]	k_2 [ml/(kg_{cat} min)]	ΔC [%]
Red. 1	22 ± 3	1834[a]	8	−0.7
Red. 2	14 ± 3	898[b]	70	−5.5
Red. 3	10 ± 3	224	175	−0.2
Red. 4	5 ± 2	78	645	−1.6

[a] Determined from a 15 min isothermal experiment at 275 °C with 40% phenol conversion.
[b] Determined from a 15 min isothermal experiment at 275 °C with 21% phenol conversion.

In our previous work [16] we developed and validated a simple kinetic model based on these two reactions to describe the HDO of phenol quantitatively by the rate constants for hydrogenation (k_1) and deoxygenation (k_2). This model will be used to quantify the experimental data in this work as well.

3. Results and discussion

3.1. Results

Ni/SiO_2 was prepared using four different preparation procedures (Red. 1–4, as described in Section 2) to investigate the effect of the metal particle size on the catalytic performance. As nickel is very prone to oxidation, the nickel particle size was analyzed in an environmental TEM after re-reduction at 450 °C and 2.5 mbar hydrogen. Fig. 2 shows selected images of each of the four catalysts and the particle size distribution. The number based average particle size of the four samples was 22 ± 3 nm, 14 ± 3 nm, 10 ± 3 nm, and 5 ± 2 nm for the catalysts Red. 1, Red. 2, Red. 3, and Red. 4, respectively. The Gaussian function fitted to the size distribution is shown to the right of the respective ETEM images in Fig. 2. Overall the four samples represent very different average particle sizes and relatively narrow particle size distributions.

The different catalysts were tested in the batch reactor setup with 50 g of phenol as reactant at 275 °C and 100 bar for 5 h. Fig. 3 shows the conversion of phenol and the yields of cyclohexane and cyclohexanol for these experiments. The conversion of phenol increased as a function of the particle size. 41% conversion of phenol was obtained for the catalyst with 5 nm Ni particles, while ca. 100% conversion was obtained for both the 14 nm and 22 nm cases. It can further be seen that the yield of cyclohexanol increased with increasing particle size, while the cyclohexane yield had a maximum for the 10 nm particle size and was lowest in the case of the largest particles. The case of the Ni/SiO_2 sample with the lowest particle size had a very high selectivity towards cyclohexane, with practically no cyclohexanol in the products.

Generally, cyclohexane and cyclohexanol constituted the main products from the reaction with a combined selectivity in the order of 80–90%. Besides these, cyclohexanone (up to 10% selectivity), cyclohexene (up to 5% selectivity), and bicyclic compounds such as dicyclohexyl ether and bicyclohexyl (up to 5% selectivity) were identified as the major byproducts. These observations support the reaction scheme in Fig. 1. As presented in Table 1, the carbon balance closed well in all experiments. Only the experiment using the catalyst Red. 2 had a loss of more than 6% carbon, but the other experiments were closed within 2%.

The data in Fig. 3 were used to fit values of k_1 and k_2 in the kinetic model introduced in the experimental section. For Red. 1 and Red. 2 (where 100% conversion was achieved during the 5 h experiments presented in Fig. 3), additional experiments of 15 min duration were performed to obtain lower conversions and allow

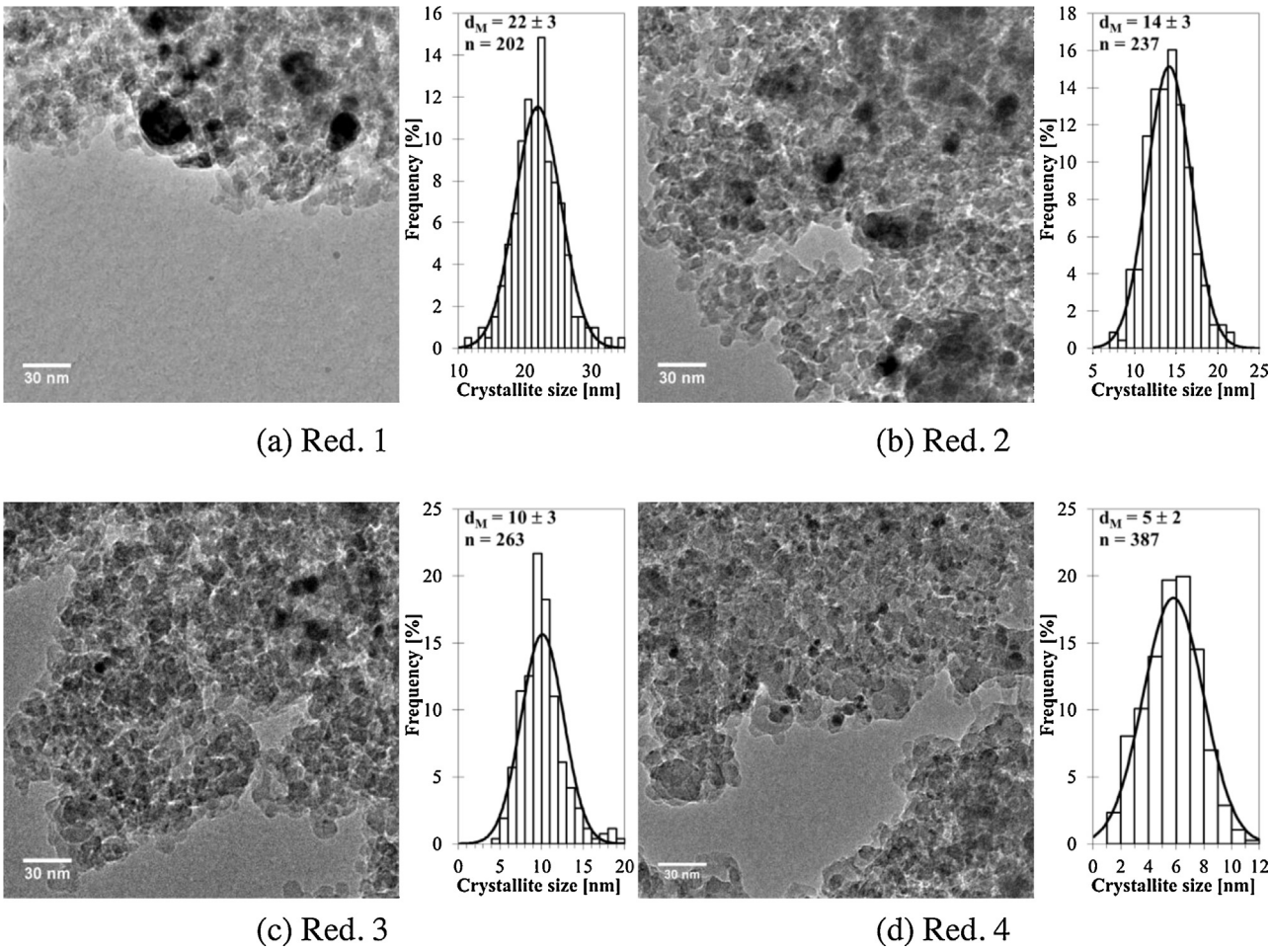

Fig. 2. Environmental transmission microscopy images of the 5 wt% Ni/SiO_2 catalysts showing particle sizes and particle size distribution and Gaussian fit of Red. 1 (a), Red. 2 (b), Red. 3 (c), and Red. 4 (d). All samples were reduced in the ETEM at 450 °C and 2.5 mbar H_2 prior to the analysis.

determination of k_1 (cf. Table 1). The rate constants are shown as a function of the nickel particle size in Fig. 4. The rate of hydrogenation (k_1) increased as a function of particle size by about two orders of magnitude from the largest to the smallest particle size. On the contrary, the rate of deoxygenation (k_2) decreased with increasing particle size. Linking these observations to Fig. 3, it follows that the low conversion of phenol to cyclohexanol for Red. 4 was accompanied by a very rapid deoxygenation, explaining the high selectivity toward cyclohexane. For this catalyst the rate constant for deoxygenation was higher than the rate constant for hydrogenation. Thus,

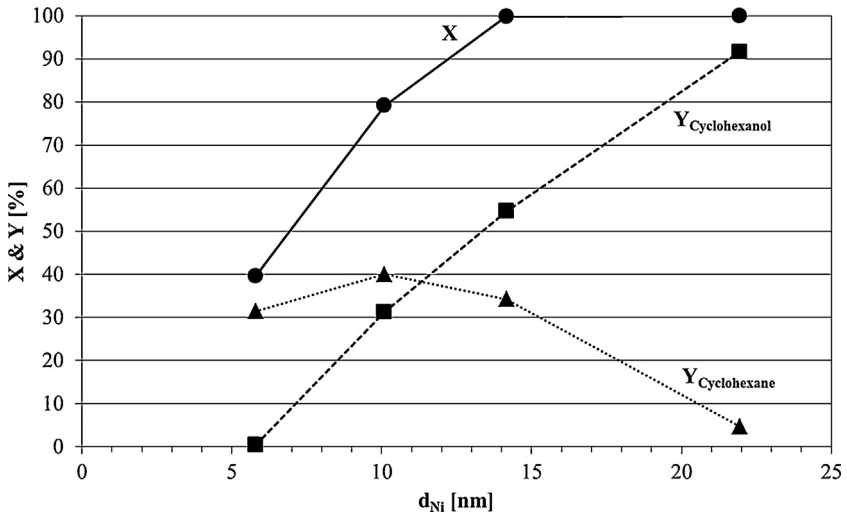

Fig. 3. Conversion of phenol (X) and yields of cyclohexanol and cyclohexane as a function of the nickel particle sizes on 5 wt% Ni/SiO_2 catalysts. The experiments were made with 1 g of catalyst in 50 g phenol. $T = 275$ °C, $P = 100$ bar, reaction time = 5 h.

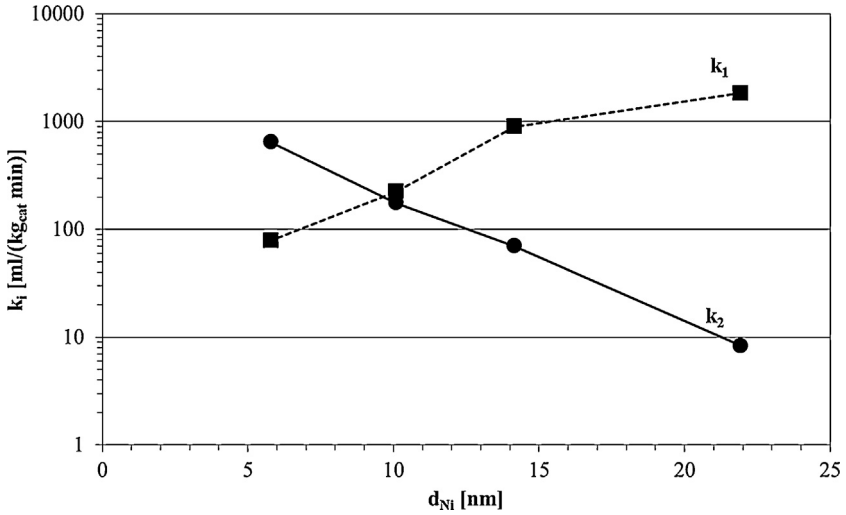

Fig. 4. k_1 and k_2 as a function of the nickel particle sizes of the 5 wt% Ni/SiO_2 catalysts. k_1 in the two cases with 100% conversion (cf. Fig. 3) was determined by additional shorter 15 min experiments. k_1 represents the rate constant for hydrogenation and k_2 represents the rate constant for deoxygenation. The experiments were made with 1 g of catalyst in 50 g phenol. Typical conditions: $T = 275\ ^\circ C$, $P = 100$ bar, reaction time = 5 h.

a shift in the rate determining step occurs for Ni/SiO_2 catalysts with nickel particles around ca. 9–10 nm, as seen from the crossing of the two curves in Fig. 4. If the particle size is above 9–10 nm, the slowest step is the deoxygenation, but below this range the hydrogenation reaction is the slowest.

3.2. Theoretical distribution of nickel sites

Further interpretation of the results in Figs. 3 and 4 requires analysis of the crystal structure and the availability of different surface sites. Three types of sites are generally considered: facet sites, step sites, and corner sites, as visualized in Fig. 5. The overall (measured) rate constant is the result of the contribution from each of these sites, leading to the following equation:

$$k = k_{facet} \cdot N_{facet} + k_{step} \cdot N_{step} + k_{corner} \cdot N_{corner} \tag{9}$$

$$\frac{k}{N_S} = k_{facet} \cdot \frac{N_{facet}}{N_S} + k_{step} \cdot \frac{N_{step}}{N_S} + k_{corner} \cdot \frac{N_{corner}}{N_S} \tag{10}$$

$$\frac{k}{N_S} = k_{facet} \cdot x_{facet} + k_{step} \cdot x_{step} + k_{corner} \cdot x_{corner} \tag{11}$$

Here k is the overall rate constant in ml/(kg_{cat} min), k_i is the rate constant at the specific site in ml/(site min), N_i is the number of sites of type i in term of sites/kg_{cat}, N_S is the total number of exposed surface atoms in sites/kg_{cat}, and x_i is the fraction of the different sites. This can be linked to the turn over frequency (TOF):

$$\mathrm{TOF} = C^\circ \cdot N_A \cdot \frac{k}{N_S} \tag{12}$$

$$\mathrm{TOF} = C^\circ \cdot N_A \cdot (k_{facet} \cdot x_{facet} + k_{step} \cdot x_{step} + k_{corner} \cdot x_{corner}) \tag{13}$$

Here TOF is the turn over frequency in s^{-1}, C° is the standard concentration of 1 mol/l (as recommended by Kozuch and Martin [33]), and N_A is the Avogadro constant in mol^{-1}. As both a rate constant for the hydrogenation reaction (k_1) and the deoxygenation reaction (k_2) have been defined, the TOF for hydrogenation (TOF_{Hyd}) and the TOF for deoxygenation (TOF_{Deox}) can now be defined on the basis of Eq. (12).

Icosahedrons are one of the preferred crystal shapes for nickel nanoparticles, as shown by Cleveland and Landman by the embedded atom method [34] and as expected for an inert support like silica where no strong metal-support interaction is expected.

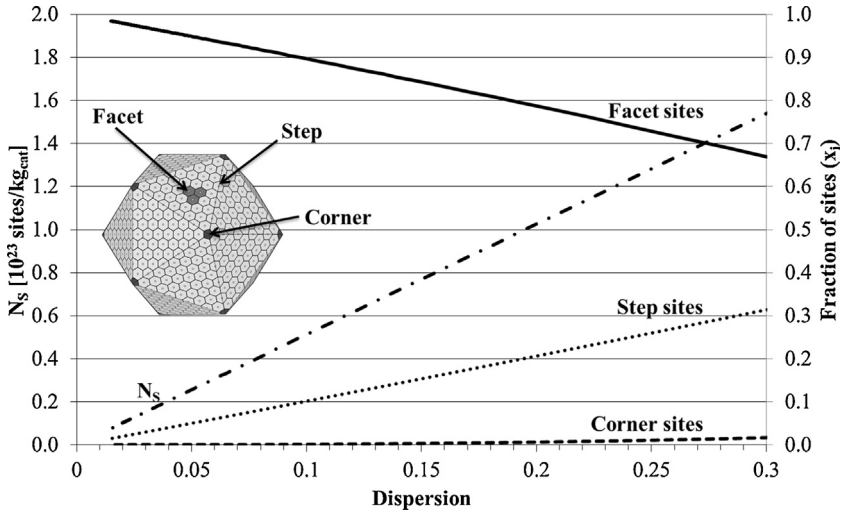

Fig. 5. Fraction of step, corner, and facet surface sites (x_i) and the total amount of surface sites (N_S) as a function of dispersion of icosahedron crystals. Calculations were made on the basis of the relations derived by Benfield [35].

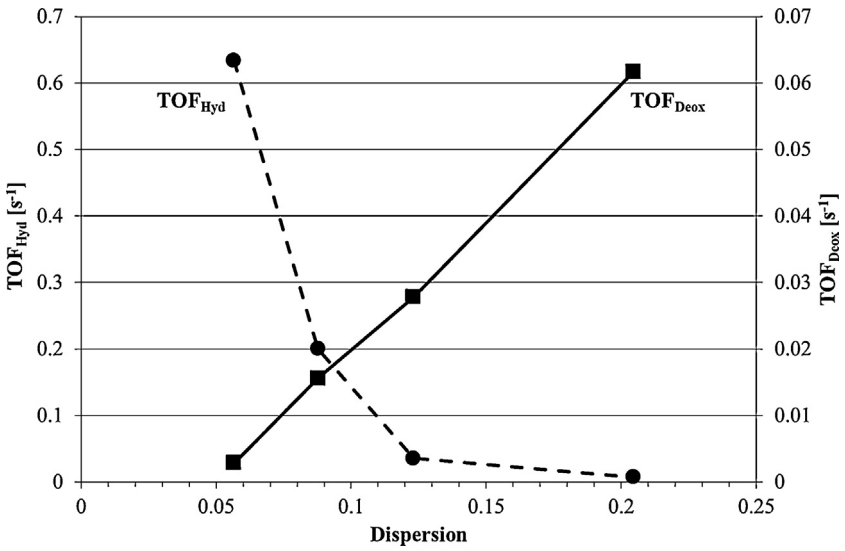

Fig. 6. TOF_{Hyd} and TOF_{Deox} over Ni/SiO_2 catalysts plotted as a function of dispersion. TOF_{Hyd} represents the TOF for hydrogenation and TOF_{Deox} represents the TOF for deoxygenation. The experiments were made with 1 g of catalyst in 50 g phenol. $T = 275\,^{\circ}C$, $P = 100$ bar, reaction time = 5 h.

The distribution of step, corner, and facet sites on an icosahedron crystal has been derived by Benfield [35] and is plotted as a function of dispersion in Fig. 5. The fraction of facet sites decreases with dispersion (approximately linearly), the fraction of step sites increases with dispersion (approximately linearly), and the fraction of corner sites slowly increases with dispersion (approximately with the square of the dispersion). Coupling this to the TOF defined in Eq. (13), shows that the TOF will decrease as a function of the dispersion if the reaction primarily is taking place on the facet sites. Contrary, the TOF will increase approximately linearly as a function of dispersion if the reaction preferentially occurs on the step sites and if the reaction preferably takes place on the corner sites it will increase with the square of the dispersion.

Additionally, the total amount of surface sites available per mass of catalyst is plotted in Fig. 5 to clearly show that the amount of available sites scales with the dispersion; at high dispersions more sites are available.

4. Discussion

On the basis of Eq. (12) and the kinetic data in Fig. 4, TOF_{Hyd} and TOF_{Deox} can be plotted as a function of dispersion, as shown in Fig. 6. TOF_{Deox} increases almost linearly as a function of dispersion. This is similar to the observed trend of the fraction of step sites in Fig. 5. As the development in the fraction of corner sites is limited in the relevant dispersion range (cf. Fig. 5), the contribution from this type of site is difficult to deduce, but most likely both step and corner sites could catalyze the reaction as both are low coordinated sites leading to the observed structure-sensitivity of the reaction. Our previous work [16] evidenced that the deoxygenation of cyclohexanol takes place by direct adsorption of the alcohol on the nickel particle, and from Fig. 6 it therefore follows that the low coordinated nickel sites facilitate the adsorption and subsequent hydrogenolysis/deoxygenation.

Structure sensitivity relations have also been observed in: steam reforming over supported noble metal and nickel catalysts [36–38], the methanation reaction over nickel catalysts [39,40], Fischer–Tropsch synthesis on cobalt and ruthenium catalysts [41–44], CO oxidation over supported gold catalysts [45–48], and CO and NO oxidation over Pt based catalysts [49], among others. Thus, structure sensitive reactions are well established. Additionally, it has also been observed for other combinations of catalysts and reactants for HDO that the rate of deoxygenation can be increased by using small particles of the active metal on supported catalysts [17,19].

Based on the experimental results and by analogy to the observations from other catalytic systems, we conclude that in the HDO process on nickel catalysts, the low-coordinated step and corner site atoms interact more readily with the oxygen group of the oxy-compound to facilitate the deoxygenation. Thus, the C—O bond breaking reaction will more readily take place on this type of site. Nevertheless, at the applied temperature, the ring still needs to be hydrogenated before the C—O bond is weak enough to be broken.

In Fig. 6, TOF_{Hyd} decreases as a function of dispersion, but not linearly. None of the surface site distributions follow a similar trend (cf. Fig. 5), indicating that this reaction is probably not directly linked to a specific type of site. At most, some similarity to the behavior of the fraction of facet sites can be drawn as this decreases linearly with dispersion.

Newman et al. [19] also observed that the surface site normalized rate of hydrogenation of phenol over a range of supported ruthenium catalysts increased with an increasing particle size of ruthenium. They suggested that large Ru particles (>ca. 10 nm) could facilitate interaction with the aromatic ring leading to its hydrogenation to cyclohexanol and subsequently cyclohexane. In our previous work [16] we have found, that hydrogenation of phenol over nickel based catalyst at temperatures below 300 °C required an oxide support. For a Ni/C catalyst, practically no conversion took place. We proposed that vacancies in the oxide support facilitated the adsorption for the phenol followed by hydrogenation by hydrogen donation from the nickel particles [16]. The present results further show that the hydrogenation of the ring is faster for large than for small particles. This may be due to simple geometric reasons, i.e. that while the phenol is adsorbed on the support it is beneficial with larger facets from which the hydrogen can be donated. It is also possible that for Ni particles of sufficient size, direct adsorption on the Ni particle becomes possible opening up a parallel path for hydrogenation relative to the small particles that require the assistance of the oxidic support. However, additional

analysis of the reaction is required to thoroughly understand the mechanism.

The rate of hydrogenation was increased by one order of magnitude by increasing the particle size (cf. Table 1), but proper choice of oxide support can lead to an increase in hydrogenation rate by several orders of magnitude [16]. Thus, proper choice of support has a larger effect when optimizing the hydrogenation rate compared to particle size.

5. Conclusion

The influence of nickel particle size for a Ni/SiO_2-based catalyst on the catalytic HDO of phenol has been investigated for particle sizes varying from 5 nm to 22 nm. A strong particle size and thus structure sensitivity was observed. Hydrogenation of the aromatic ring to form cyclohexanol was required before deoxygenation could take place. The large particles were observed to be very active for hydrogenation of phenol, giving 100% conversion of phenol into primarily cyclohexanol in 5 h reaction time at 275 °C. By decreasing the particle size the conversion of phenol decreased and the yield of cyclohexane increased, reaching a maximum yield of 38% for a catalyst with a nickel particle size of 10 nm.

A simple kinetic model was set up to analyze the observations from the experiments quantitatively in terms of hydrogenation and deoxygenation rate constants. The model showed that the rate of hydrogenation increased with increasing particle size (decreasing dispersion) while the opposite trend was observed for the deoxygenation step. The rate determining step thus changed at about 9–10 nm, where hydrogenation was the slower step for particles below 9–10 nm while the deoxygenation step was rate-limiting above this size. Thus, to achieve a high yield of the deoxygenated product cyclohexane, good control of the particle size is needed and a size of 9–10 nm seems optimal.

Comparison of the TOF for the deoxygenation reaction with that calculated from surface site population theory for the nickel particles led to the conclusion that the rate of deoxygenation was linked to the fraction of available step sites on the nickel particles. This reaction therefore more readily took place on small nickel particles. Probably, both the adsorption of the oxy-compound and the C—O bond cleavage more readily occurs on a low coordinated nickel atom.

Hydrogenation of the aromatic ring occurred best on large nickel particles (>10 nm). This is possibly due to faster hydrogenation of the benzene ring from the larger facets while the phenol is attached to the support, or that phenol can adsorp directly and become hydrogenated on the large particles, opening up a parallel path for hydrogenation. If nickel is present as small nickel nanoparticles (less than ca. 10 nm), an oxidic support is required to assist in the adsorption and hydrogenation of phenol.

Overall it is concluded that an intermediate nickel particle size is needed for optimal phenol HDO over Ni/SiO_2 at temperature below 300 °C. Relatively small particles are required to facilitate deoxygenation, but too small particles will have lower activity for hydrogenation which will hinder the overall degree of deoxygenation.

Acknowledgements

This work is part of the Combustion and Harmful Emission Control (CHEC) research center at the Department of Chemical and Biochemical Engineering at the Technical University of Denmark (DTU). The present work is financed by DTU and the Catalysis for Sustainable Energy initiative (CASE), funded by the Danish Ministry of Science, Technology and Innovation.

We thank Thomas Willum Hansen from Center for Electron Nanoscopy (CEN) at DTU for assistance with the ETEM measurements and interpretation.

Appendix A. Supplementary data

Supplementary data associated with this article can be found, in the online version, at http://dx.doi.org/10.1016/j.cattod.2015.08.022.

References

[1] P.M. Mortensen, J.-D. Grunwaldt, P.A. Jensen, K.G. Knudsen, A.D. Jensen, Appl. Catal. A: Gen. 407 (2011) 1–19.
[2] T. Bridgwater, J. Sci. Food Agric. 86 (2006) 1755–1768.
[3] Q. Zhang, J. Chang, T. Wang, Y. Xu, Energy Convers. Manag. 48 (2007) 87–92.
[4] A.V. Bridgwater, S. Czernik, J. Diebold, D. Meier, A. Oasmaa, C. Peakocke, J. Piskorz, D. Radlein, Fast Pyrolysis of Biomass: A Handbook, CPL Press, Newbury, 1999.
[5] E. Furimsky, Appl. Catal. A: Gen. 199 (2000) 144–190.
[6] P. Grange, E. Laurent, R. Maggi, A. Centeno, B. Delmon, Catal. Today 29 (1996) 297–301.
[7] R.H. Venderbosch, A.R. Ardiyanti, J. Wildschut, A. Oasmaa, H.J. Heeres, J. Chem. Technol. Biotechnol. 85 (2010) 674–686.
[8] M.S.A. Moraes, M.V. Migliorini, F.C. Damasceno, F. Georges, S. Almeida, C.A. Zini, R.A. Jacques, E.B. Caramão, J. Anal. Appl. Pyrolysis 98 (2012) 51–64.
[9] Q. Bu, H. Lei, A.H. Zacher, L. Wang, S. Ren, J. Liang, Y. Wei, Y. Liu, J. Tang, Q. Zhang, R. Ruan, Bioresour. Technol. 124 (2012) 470–477.
[10] V.A. Yakovlev, S.A. Khromova, O.V. Sherstyuk, V.O. Dundich, D.Y. Ermakov, V.M. Novopashina, M.Y. Lebedev, O. Bulavchenko, V.N. Parmon, Catal. Today 144 (2009) 362–366.
[11] A.R. Adriyanti, S.A. Khromova, R.H. Venderbosch, V.A. Yakovlev, H.J. Heeres, Appl. Catal. B: Environ. 117–118 (2012) 105–117.
[12] M.V. Bykova, O.A. Bulavchenko, D.Y. Ermakov, M.Y. Lebedev, V.A. Yakovlev, V.N. Parmon, Biocatalysis 3 (2011) 15–22.
[13] M.V. Bykova, D.Y. Ermakov, V.V. Kaichev, O. Bulavchenko, A.A. Saraev, M.Y. Lebedev, V.A. Yakovlev, Appl. Catal. B: Environ. 113–114 (2012) 296–307.
[14] M.V. Bykova, S.G. Zavarukhin, L.I. Trusov, V.A. Yakovlev, Kinet. Catal. 54 (2013) 40–48.
[15] V.O. Dundich, S.A. Khromova, D.Y. Ermakov, M.Y. Lebedev, V.M. Novopashina, V.G. Sister, A.I. Yakimchuk, V.A. Yakovlev, Kinet. Catal. 51 (2010) 728–734.
[16] P.M. Mortensen, J.-D. Grunwaldt, P.A. Jensen, A.D. Jensen, ACS Catal. 3 (2013) 1774–1785.
[17] P.M. Mortensen, D. Gardini, H.W.P. de Carvalho, C.D. Damsgaard, J.-D. Grunwaldt, P.A. Jensen, J.B. Wagner, A.D. Jensen, Catal. Sci. Technol. 4 (2014) 3672–3686.
[18] N. Shuikin, L. Erivanskaya, Russ. Chem. Rev. 29 (1960) 309–320.
[19] C. Newman, X. Zhou, B. Goundie, I.T. Ghampson, R.A. Pollock, Z. Ross, M.C. Wheeler, R.W. Meulenberg, R.N. Austin, B.G. Frederick, Appl. Catal. A: Gen. 477 (2014) 64–74.
[20] C. Zhao, J. He, A.A. Lemonidou, X. Li, J.A. Lercher, J. Catal. 280 (2011) 8–16.
[21] C. Zhao, Y. Kuo, A.A. Lemonidou, X. Li, J.A. Lercher, Angew. Chem. Int. Ed. 48 (2009) 3987–3990.
[22] H. Ohta, H. Kobayashi, K. Hara, A. Fukuoka, Chem. Commun. 47 (2011) 12209–12211.
[23] C. Zhao, S. Kasakov, J. He, J.A. Lercher, J. Catal. 296 (2012) 12–23.
[24] E.-M. Ryymin, M.L. Honkela, T.-R. Viljava, A.O.I. Krause, Appl. Catal. A: Gen. 389 (2010) 114–121.
[25] C.H. Bartholomew, Appl. Catal. A: Gen. 107 (1993) 1–57.
[26] J. Sehested, J. Catal. 217 (2003) 417–426.
[27] J. Sehested, Catal. Today 111 (2006) 103–110.
[28] C. Louis, Z.X. Cheng, M. Che, J. Phys. Chem. 97 (1993) 5703–5712.
[29] H.S. Fogler, Elements of Chemical Reaction Engineering, Prentice Hall, New Jersey, 2006.
[30] K. Schofield, Prog. Energy Combust. Sci. 34 (2008) 330–350.
[31] P.L. Llewellyn, E. Bloch, S. Bourelly, Characterization of Solid Material and Heterogenous Catalysts, Wiley-VCH, Weinheim, 2012, pp. 853–880.
[32] A. Borodzinski, M. Bonarowska, Langmuir 13 (1997) 5613–5620.
[33] S. Kozuch, J.M.L. Martin, ACS Catal. 2 (2012) 2787–2794.
[34] C.L. Cleveland, U. Landman, J. Chem. Phys. 94 (1991) 7376–7396.
[35] R.E. Benfield, J. Chem. Soc. Faraday Trans. 88 (1992) 1107–1110.
[36] G. Jones, J.G. Jakobsen, S.S. Shim, J. Kleis, M.P. Andersson, J. Rossmeisl, F. Abild-Pedersen, T. Bligaard, S. Helveg, B. Hinnemann, J.R. Rostrup-Nielsen, I. Chorkendorff, J. Sehested, J.K. Nørskov, J. Catal. 259 (2008) 147–160.
[37] D.A.J.M. Lighthart, R.A. van Santen, E.J.M. Hensen, J. Catal. 280 (2011) 206–220.
[38] J. Wei, E. Iglesia, J. Phys. Chem. B 108 (2004) 4094–4103.
[39] J. Engbæk, O. Lytken, J.H. Nielsen, I. Chorkendorff, Surf. Sci 602 (2008) 733–743.
[40] M.P. Andersson, F. Abild-Pedersen, I.N. Remediakis, T. Bligaard, G. Jones, J. Engbæk, O. Lytken, S. Horch, J.H. Nielsen, J. Sehested, J.R. Rostrup-Nielsen, J.K. Nørskov, I. Chork-endorff, J. Catal. 255 (2008) 6–19.

[41] V. Ragaini, R. Carli, C.L. Bianchi, D. Lorenzetti, G. Predieri, P. Moggi, Appl. Catal. A: Gen. 139 (1996) 31–42.
[42] J.P. den Breejen, P.B. Radstake, G.L. Bezemer, J.H. Bitter, V. Frøseth, A. Holmen, K.P. de Jong, J. Am. Chem. Soc. 131 (2009) 7197–7203.
[43] J. Yang, E.Z. Tveten, D. Chen, A. Holmen, Langmuir 26 (2010) 16558–16567.
[44] J.M.G. Carballo, J. Yang, A. Holmen, S. García-Rodríguez, S. Rojas, M. Ojeda, J.L.G. Fierro, J. Catal. 284 (2011) 102–108.
[45] J.-D. Grunwaldt, M. Maciejewski, O.S. Becker, P. Fabrizioli, A. Baiker, J. Catal. 186 (1999) 458–469.
[46] B. Hvolbæk, T.V.W. Janssens, B.S. Clausen, H. Falsig, C.H. Christensen, J.K. Nørskov, Nanotoday 2 (2007) 14–18.
[47] T.V.W. Janssens, A. Carlsson, A. Puig-Molina, B.S. Clausen, J. Catal. 240 (2006) 108–113.
[48] N. Lopez, J.K. Nørskov, T.V.W. Janssens, A. Carlsson, A. Puig-Molina, B.S. Clausen, J.-D. Grunwaldt, J. Catal. 225 (2004) 86.
[49] A. Boubnov, S. Dahl, E. Johnson, A.P. Molina, S.B. Simonsen, F.M. Cano, S. Helveg, L.J. Lemus-Yegres, J.-D. Grunwaldt, Appl. Catal. B: Environ. 126 (2012) 315–325.